Tunable enhancement of light absorption and scattering in $Si_{1-x}Ge_x$ nanowires

Houssem Kallel,[1,2,3,*] Arnaud Arbouet,[1,2] Gérard BenAssayag,[2] Abdallah Chehaidar,[3] Alexis Potié,[4] Bassem Salem,[4] Thierry Baron,[4] and Vincent Paillard[1,2,†]

[1]*Université de Toulouse, Université Paul Sabatier, 118 route de Narbonne, 31062 Toulouse cedex 9, France*
[2]*CEMES-CNRS, 29 rue Jeanne Marvig, 31055 Toulouse Cedex 4, France*
[3]*Départment de Physique, Faculté des Sciences de Sfax, Université de Sfax, BP 1171, 3000 Sfax, Tunisia*
[4]*LTM/CNRS-CEA-LETI, 17 rue des martyrs, 38054 Grenoble, France*

Semiconducting nanowires (NWs) are good candidates for new optoelectronic or photovoltaic devices due to their excellent ability to guide, scatter, or absorb light, from near ultraviolet to near infrared. The existence of morphology-dependent optical resonances opens a promising route to overcome the intrinsic limitations of the constituent material and optimize their interaction with light. We propose a thorough investigation of the optical properties of $Si_{1-x}Ge_x$ alloy nanowires addressing the influence of NW diameter, composition, light polarization, and angle of incidence on their scattering and absorption. Our results clearly show that the Ge composition provides an additional degree of freedom to tailor the optical response of these one-dimensional nano-objects and that resonant enhancement of both absorption and scattering can be obtained in the infrared range at relatively small diameters compared to pure Si nanowires. These results are confirmed by complementary light scattering and Raman spectroscopy experiments using confocal dark field optical microscopy on individual nanowires fabricated by Au-catalyzed vapor-liquid-solid synthesis.

I. INTRODUCTION

Semiconductor nanowires have attracted much attention in the last decade for their original optical and electronic properties. This intense research work has led these one-dimensional nanostructures at the heart of next-generation architectures of sensors, photovoltaic devices, photodetectors, and transistors.[1–3] Despite the supremacy of silicon in microelectronics or low cost solar cells, its poor intrinsic optical properties have so far precluded its massive use in optoelectronics. Recent elastic light-scattering experiments and photocurrent measurements have demonstrated that the optical response of subwavelength silicon and germanium nanowires can be dramatically enhanced at some specific wavelengths.[4–8] Considering these nano-objects as ultimately downscaled cylindrical waveguides, the existence of these morphology-dependent optical resonances has been ascribed to the excitation of so-called leaky optical modes similar to the optical resonances of cylindrical cavities or microdisk resonators. These leaky mode resonances (LMRs) occur whenever the electric-field intensity can build up inside the high refractive index nano-object due to constructive interference after multiple round trips inside the NW perimeter. This resonant enhancement compensates the poor intrinsic optical properties of silicon inherited from its indirect band gap. It should be noticed that the first publication on the subject, to the best of our knowledge, was dedicated to the explanation of the high-temperature optical annealing of Si nanowires (NWs) illuminated by visible light, in apparent contradiction with the low extinction coefficient of Si in this wavelength range.[9] Numerical simulations and experiments have recently been performed on either germanium[5] or silicon nanowires.[7,8] These investigations have shown that, in the spectral range where these materials have a low extinction coefficient, resonant effects due to the excitation of LMRs inside the nanowire show off at specific wavelengths arranged on complex (λ,d) maps.[7,8]

This enhanced interaction with light compared to the bulk opens the route towards the use of semiconductor nanowires in solar cells or photodetectors in order to improve their efficiency, while decreasing their cost. Due to its lower band gap, germanium is currently used as the bottom junction in high efficiency multijunction solar cells to increase light harvesting in the infrared part of the light spectrum. Because of its higher cost, the use of germanium is today mostly limited to demanding applications such as space applications. Thus NW-based solar cells could achieve high efficiency at low cost since only a small volume of lower quality material is needed. Indeed, the low optical absorption of bulk silicon or germanium imposes the use of thick films to absorb incident photons. Therefore excellent crystalline quality ensuring large charge diffusion lengths is required to maximize the solar cell efficiency. The carrier diffusion length is less important in NWs where core-shell geometry leads to much smaller distances between the photogeneration and the collection of carriers. The photocurrent enhancement has already been demonstrated in the case of single silicon or germanium nanowires that could be used as single photovoltaic element or on-chip photodetectors.[5,10]

Finally, the enhanced interaction of nanowires with light is interesting for Raman scattering experiments. The Raman response of the NW can be enhanced when the excitation wavelength matches a LMR mode, and even more when the LMR is also corresponding to an electronic resonance.[11–13] The local-field enhancement on the nanowire can also be used to detect molecules or nanoparticles located in the near field of the nanowire.[14] However, the resonant effects may be difficult to obtain by adjusting the NW diameter only. For instance, infrared resonances can be obtained using Si NWs for diameters much larger than 200 nm,[8] which could be an issue for low cost photovoltaic devices, while the most efficient absorption resonances in the UV-blue range are difficult to obtain with germanium NWs (diameters smaller than 30 nm).[5]
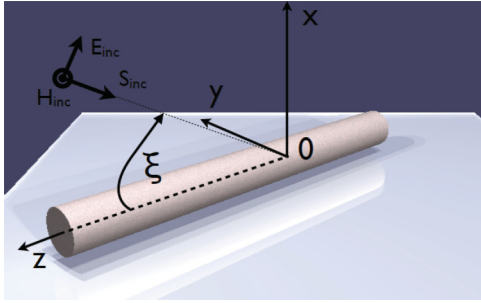
FIG. 1. (Color online) Schematic geometry of light scattering by a cylinder. The finite length and the substrate correspond to the experimental case.

In this context, in order to limit the NW diameter to a few tenths to the hundred of nm, we investigated light scattering and absorption by $Si_{1-x}Ge_x$ alloy nanowires and showed that the composition x of germanium provides an additional degree of freedom to optimize their light absorption and scattering from the ultraviolet to the infrared. In this latter range, our results show that significant enhancements are obtained at relatively small diameters. First, numerical simulations realized in the framework of Lorenz-Mie formalism are presented and evidence the LMRs of $Si_{1-x}Ge_x$ alloy nanowires. The impact of nanowire diameter, composition, and incidence angle are carefully addressed. These theoretical results are confirmed by complementary confocal elastic light scattering and Raman spectroscopy experiments on individual nanowires, grown by Au-catalyzed vapor-liquid-solid synthesis (VLS).

II. LIGHT SCATTERING AND ABSORPTION EFFICIENCIES OF $Si_{1-x}Ge_x$ NANOWIRES

To quantitatively predict light absorption and scattering by $Si_{1-x}Ge_x$, we used the Lorenz-Mie theory. In this framework, a nanowire is described as an infinitely long cylinder dispersed in a nonabsorbing, linear, homogeneous, and isotropic medium.[9,15] A schematic view is given in Fig. 1.

The absorption and scattering efficiencies, respectively noted Q_{abs} and Q_{sca}, are dimensionless values defined as the ratio of the absorption or scattering cross section to the geometrical cross section of the nanowire (see Appendix subsection 1). In the following, the influence of the nanowire diameter and composition as well as the incident electric-field wavelength and polarization are investigated. The transverse electric (TE) [respectively transverse magnetic (TM)] mode refers to an electric field perpendicular to (respectively contained in) the incidence plane, the latter being defined by the nanowire axis and incident wave vector. The unpolarized (UP) configuration corresponds to the average of TE and TM configurations, which gives for the scattering efficiency $Q_{sca}^{UP} = \frac{1}{2}(Q_{sca}^{TM} + Q_{sca}^{TE})$. We also addressed the impact of the angle of incidence ξ between the incident wave vector k_{inc} and the nanowire axis.

The complex refractive index

$$\eta_2 = n_2 + i\kappa_2 \tag{1}$$

for any alloy composition was assumed to be that of relaxed bulk $Si_{1-x}Ge_x$. Missing data were interpolated from the optical constants measured by Humlíček and co-workers.[16,17] The optical constants of $Si_{1-x}Ge_x$ alloys can be found in Appendix subsection 2. In the following, the scattering and absorption efficiencies are represented in two-dimensional color maps, as a function of wavelength and nanowire diameter. Our calculations are given for diameters in the 10–250-nm range corresponding to NWs grown by the VLS technique. Given the exciton Bohr radius of silicon and germanium, quantum size effects are expected to play a significant role only for diameters smaller than 30 nm.[18] Even if these effects have been neglected in our calculations, our results allow us to understand the influence of the nanowire morphology even below this limit.

Figure 2 presents Q_{abs} and Q_{sca} for unpolarized excitation at normal incidence ($\xi = 90°$) for different $Si_{1-x}Ge_x$ alloy compositions. The results for TE and TM configurations are presented in Appendix subsection 3. Both scattering and absorption efficiencies are strongly polarization dependent. Our results for pure Si and pure Ge are in very good agreement with those published by Cao and co-workers[6,7] and Brönstrup *et al.*[8]

Above a composition-dependent wavelength threshold visible as a vertical white line in Fig. 2 in the case of $Si_{50}Ge_{50}$, the results for Q_{abs} and Q_{sca} show large similarities and clearly evidence strong optical resonances distributed on a complex branched structure. Care must be taken that the color bars for scattering and absorption efficiencies are different, light being
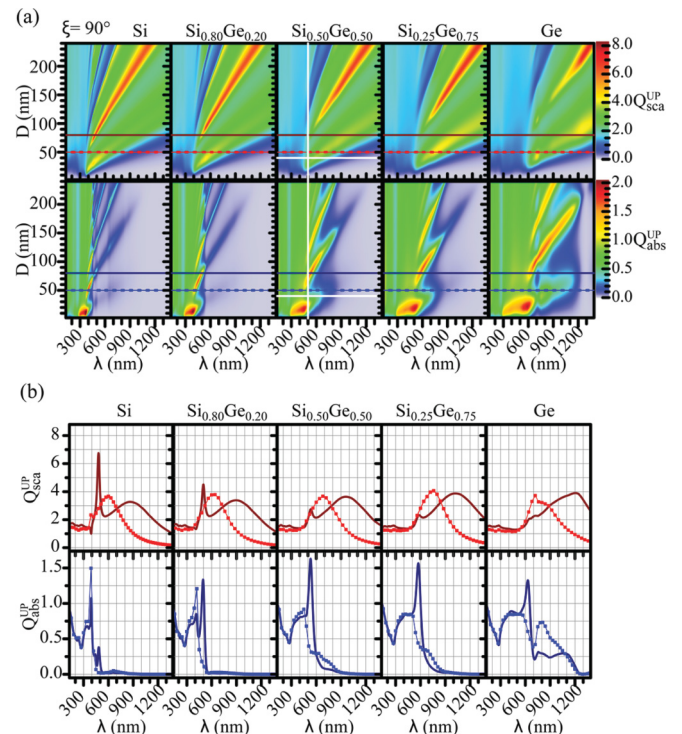

FIG. 2. (Color online) (a) Absorption and scattering efficiencies of a $Si_{1-x}Ge_x$ NW in vacuum as a function of diameter and wavelength of incident light for different germanium compositions x. The incident wave vector is perpendicular to the cylinder axis. The vertical and horizontal white lines give specific thresholds (see text). (b) Scattering efficiency Q_{sca} and absorption efficiency Q_{abs} as a function of x for two NW diameters (75 nm, solid lines, and 50 nm, dotted lines)

predominantly scattered by the NW in the considered spectral range.

Above this wavelength threshold, the NW material is nonabsorbing with an extinction coefficient κ_2 much lower than 1, while its refractive index n_2 is high enough to allow light trapping inside the nanowire by decreasing the effective optical wavelength from its value in vacuum (300–1200 nm) down to the NW diameter range (10–100 nm). Figure 2 shows that the wavelength threshold is redshifted with increasing composition x of germanium. This is consistent with the redshift of the high absorption region (high κ) of $Si_{1-x}Ge_x$ alloys with increasing x (see Appendix subsection 2).

More quantitatively, the onset of the LMRs shifts from about 380 nm in Si to about 620 nm in Ge.[16,17] The resonances apparent above this threshold are similar to those of microdisk resonators or cylindrical cavities and are identified as leaky mode resonances in optical fibers and other dielectric resonators. They are highly confined and occur whenever light can be trapped inside the nanowire by multiple reflections on the nanowire-surrounding medium interface.[5,19] This constructive interference condition requires that an integer number m of the effective optical wavelength fits into the nanowire perimeter: $\pi D \approx m\lambda/n_2$. Obviously, thicker nanowires can sustain several different LMRs.

The optical resonances are arranged on nearly straight lines in the (λ, d) maps due to the nearly constant value of the refractive index of $Si_{1-x}Ge_x$ above the wavelength threshold. Whereas most strategies to develop nanowire-based devices involve a change in diameter to meet the resonance condition, our results show that the latter can alternatively be satisfied by a proper choice of the alloy composition. Our results show that increasing the Ge composition x induces a redshift of the LMRs consistent with the redshift of the refractive index curves from pure Si to pure Ge (see Appendix subsection 2). Therefore $Si_{1-x}Ge_x$ alloy nanowires display resonantly enhanced interaction with light that can be tuned by a proper choice of the Ge composition x. Resonances can be also easily observed from the spectra in Fig. 2(b).

Below the wavelength threshold (left of vertical white line in Fig. 2), the optical properties of the $Si_{1-x}Ge_x$ nanowires are dominated by their strong absorption due to direct electronic transitions from the valence band to the conduction band. This yields very short light absorption lengths that undermine the multiple reflections at the origin of the resonant enhancement of the electric field inside the NW. As a consequence, only one LMR survives in the thinnest nanowires that can be ascribed to the fundamental mode TM_{01}.[6] This resonance is further reinforced by the intrinsic absorption of the material associated with direct electronic transitions. The latter explains why the maximum value of Q_{abs} in Si corresponds to the E_0 and E_1 transitions located at 364 and 295 nm, respectively. The Q_{abs} maximum region is spread over a wider range of wavelengths with increasing concentration of Ge, according to the degeneracy lifting of E_0', E_1, $E_1 + \Delta_1$, $E_0 + \Delta_0$, and E_0.[20] It must be remarked that the existence of a clear maximum of the absorption efficiency below the wavelength threshold is specific to small diameter nanowires. It is not observed in the case of a silicon slab of the same thickness as the NW diameter. The absorbance calculations (not shown) for Si slabs thinner than 40 nm exhibit roughly the same branched

structure as shown for nanowires, but display a nearly uniform and weak absorbance, without any optical resonance, below the wavelength threshold. This specific behavior is due to the particular strength of the optical resonances in the case of nanowires.

To go further, we investigate the dependence of scattering and absorption efficiencies with angle of incidence ξ for different Ge concentrations x. This issue is important as optical spectroscopy using a tightly focused light beam through a high numerical aperture (NA) microscope objective can involve low ξ angles, thus incident wave vectors k_{inc} nearly parallel to the nanowire axis (see Fig. 1). The LMRs at the origin of the optical response enhancement at specific wavelengths arise from constructive interference in transverse planes of the NWs. The excitation efficiency of LMRs will therefore depend upon the magnitude of the projection $k_{inc\perp}$ of the incident wave vector k_{inc} perpendicular to the NW axis.

Figure 3 shows the angular dependence for different Ge concentrations x and for three diameters ($D_1 = 20$ nm, $D_2 = 50$ nm, and $D_3 = 100$ nm). Figure 3(a) shows that in small NWs (D_1), in which the optical response is governed by a single TM_{01} LMR, light incident at low angle ξ poorly couples to the LMR, whereas increasing $k_{inc\perp}$ by either increasing the incidence angle or decreasing the wavelength can boost the absorption and scattering efficiencies of the nanowire by exciting this TM_{01} mode. This still holds for $D_2 = 50$ nm, whereas for larger diameters (D_3) the situation becomes slightly more complex as several degenerate LMRs can be excited.

For the smallest diameter D_1, there is a sharp transition for angles smaller than 40° for Q_{sca} or 30° for Q_{abs}. These efficiencies do not change significantly for incident angles decreasing from normal incidence ($\xi = 90°$) down to the above-mentioned limits, and are negligible beyond these limits. The case of the other diameters D_2 and D_3 differs noticeably: the scattering efficiency can remain high at low incidence angle, and more importantly the wavelength at which Q_{sca} is maximum depends upon the incidence angle.[8] For instance, in the case of D_3, the Q_{sca} maximum at small incidence angles (about 450–500% at 20°) is redshifted by about 50 nm at larger incidence angles (about 450–500% from 35° to 90°), for all Ge composition x. Thus the scattered light spectrum (or the color) of a 20-nm nanowire in a tightly focused light spot composed of a wide range of wave vectors is not expected to be different from the color of the same nanowire under normal incidence. On the contrary, the color of larger nanowires will depend upon its illumination. In fact, the angular dependence should not be an issue for a photovoltaic device since resonances are roughly angle independent except for small diameter NWs having lower efficiencies for low incidence angles. However, the variations observed as a function of the parameters ξ and D could be very important for the interpretation of experimental results on isolated nanowires such as presented in this work.

Our results show that the strong optical resonances in $Si_{1-x}Ge_x$ nanowires can be tuned via the composition x, which is a very interesting way to optimize both light scattering and absorption in solar cells or photodetectors.[5] This enhanced light-matter interaction is also very important for enhanced Raman scattering from and by nanowires.[11,12] Though the
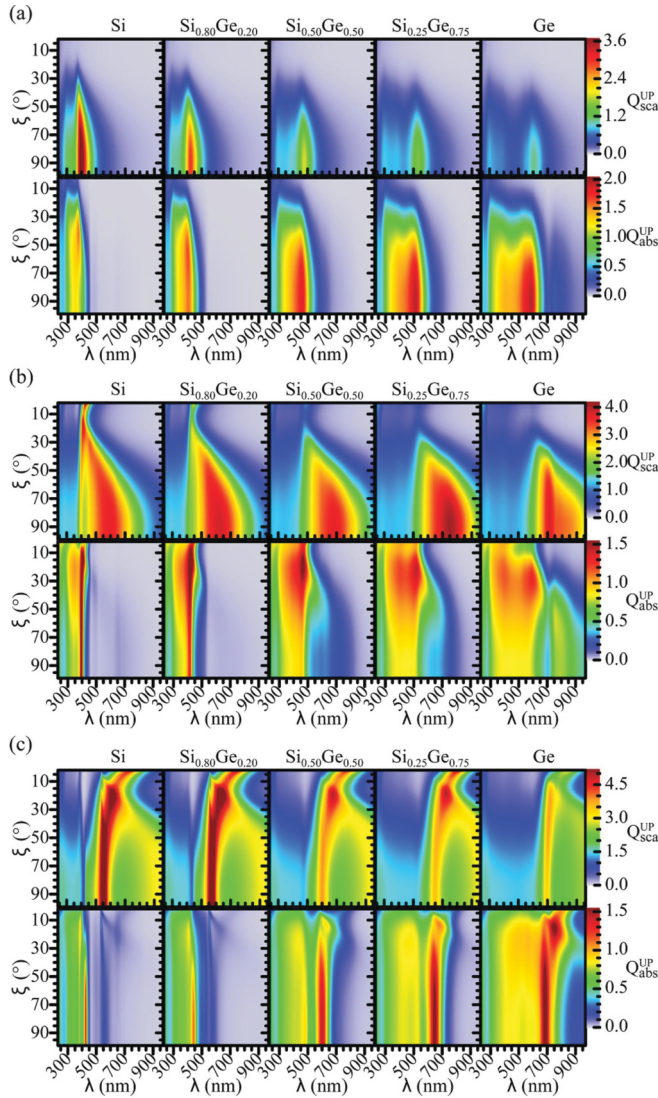
FIG. 3. (Color online) Absorption and scattering efficiencies for three nanowire diameters and different germanium compositions x as a function of the incidence angle ξ and the incident wavelength. The surrounding medium is vaccuum. (a) $D_1 = 20$ nm, (b) $D_2 = 50$ nm, (c) $D_3 = 100$ nm.
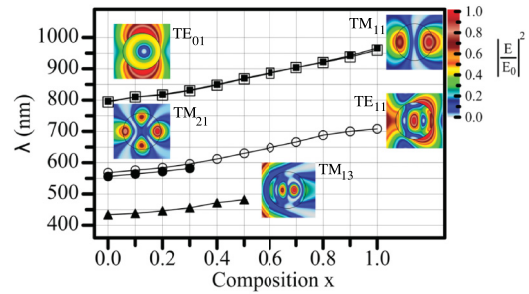

FIG. 4. (Color online) LMR wavelength for different germanium composition x. The nanowire diameter is 160 nm. The corresponding normalized electric-field intensity for each mode is given in inset. Some modes exist only on a limited composition range.

influence of Ge composition can be seen in the previous (λ, d) maps of Fig. 2, we have extracted and identified the different LMRs and plotted their position as a function of x for a given diameter. The results presented in Fig. 4 show that a very broad spectral range is accessible by simply adjusting the germanium content.

In the following, we present optical spectroscopy experiments on individual NWs to evidence the resonances of $Si_{1-x}Ge_x$ NWs of known composition and morphology.

III. OPTICAL SPECTROSCOPY OF INDIVIDUAL $Si_{1-x}Ge_x$

The $Si_{1-x}Ge_x$ NWs were grown in a hot-wall reduced pressure chemical vapor deposition (RP-CVD) system via the VLS process. The total pressure was around 4.5 Torr and hydrogen was used as a carrier gas. Si and Ge are provided by pure silane (SiH_4) and diluted germane in hydrogen

(10% GeH_4 in H_2). First, a 2-nm-thick Au layer was deposited on Si (111) substrates. The substrate was then loaded in the deposition chamber and annealed at 650 °C for several minutes in order to form Au nanodroplets. Following droplet formation, the temperature was cooled down to the deposition temperature, typically between 325 and 450 °C. The samples were then exposed to the reactive gases (SiH_4, GeH_4). The gas ratio (GeH_4 flux over SiH_4 flux), pressure, and temperature were adjusted to control the Ge content in NWs, and HCl was added to the gas mixture to optimize the NWs physical properties.[21,22]

The gold nanoparticle was then removed and nanowire solutions were obtained by dilution and sonication in isopropanol. Isolated nanowires were drop coated on a Si (001)-oriented substrate, except for pure Si-NWs deposited on a glass substrate. It has recently been shown that the color of individual NWs on glass in dark field images can provide an estimation of the NW size.[7,8] Preliminary experiments on pure Si-NWs gave results in very good agreement with those published by Brönstrup *et al.*[8] Compared to a glass substrate, the choice of a silicon substrate was made because it is conductive enough to allow focused ion beam (FIB) and scanning electron microscopy (SEM) experiments, ensuring size and optical measurements on the same nanowire. The (001)-Si substrate also exhibits a phonon spectrum that can be eliminated thanks to Raman selection rules (thus allowing nanowire detection), and it is a good thermal conductor limiting excessive heating.

A typical example of isolated nanowires is shown in Fig. 5. Reference marks are etched by FIB for subsequent localization of individual NWs by optical microscopy. The NW diameters are measured by SEM. The optical spectroscopy experiments are performed on a customized confocal optical microscope (Horiba-Jobin Yvon Xplora MV2000) allowing Raman spectrometry, dark field scattering spectroscopy and imaging. The confocal microscope with a $100\times$, 0.9 numerical aperture (NA), BF/DF objective is used in bright field (BF) configuration to record Raman spectra with different excitations (532, 633, and 785 nm) and gratings (from 600 to 2400 groves/mm). The dark field (DF) scattering spectra are collected with a $50\times$, 0.6-NA, BF/DF objective, a halogen lamp, and a 300 groves/mm grating. The use of a limited NA is necessary to prevent angles far from normal incidence, since low angles could affect the results for some NW diameters as described in the previous section. Under the
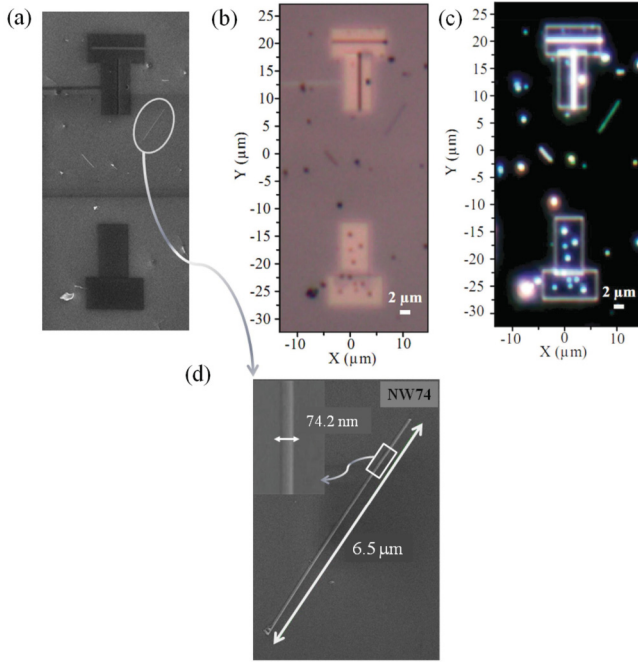
FIG. 5. (Color online) (a) SEM image showing the FIB marks and isolated nanowires. Optical bright field (b) and dark field (c) images of the same region. (d) SEM measurement of the dimensions of an isolated nanowire.

FIG. 6. (Color online) Raman spectra recorded on and outside the nanowire NW49 in different Raman configurations. The $Z(X'Y')\bar{Z}$ configuration (labeled crossed config. in the inset) is used to remove the Si substrate contribution. Z, X', and Y' correspond to, respectively, [001], [1$\bar{1}$0], and [110] substrate crystallographic directions.

optical microscope, the reference marks are easily observed in bright field. They give a very weak scattering in dark field and therefore do not affect the scattering spectra of the neighboring nanowires. This system, coupled to localization marks, allows us to make inelastic and elastic light-scattering measurements on the same nanowire (which size is known).

In the following, we discuss the results obtained on typical $Si_{1-x}Ge_x$ NWs having a nominal composition of $x = 20\%$ and $x = 55\%$, according to growth conditions, and various diameters.

Composition and structure of isolated nanowires can be determined using Raman spectroscopy.[23] Preliminary tests were performed to assess the maximum admissible power for a 532-nm excitation focused through a $100\times$, 0.9-NA microscope objective, that allows neglecting any temperature effect on the isolated nanowires. This point was crucial because the 532-nm excitation can be strongly absorbed due to near-resonant Raman conditions for Ge compositions x ranging from 0.4 to 0.55. We found that a power of 100 μW on the sample was an upper limit in the case of NWs deposited on a single-crystal silicon. Raman spectra were also recorded in different configurations to eliminate most of the contribution from the (001)-oriented Si substrate, especially the LO phonon at 521 cm^{-1} and the 2TA singularity around 300 cm^{-1}. We assumed strain-free NWs and neglected any phonon confinement effect; the wave number shifts are therefore attributed to the variation in Ge composition. Typical spectra are given in Fig. 6.

The Ge composition x can be accurately determined from the wave number of the different optical phonons corresponding to Si-Si and Ge-Ge vibration modes, using the
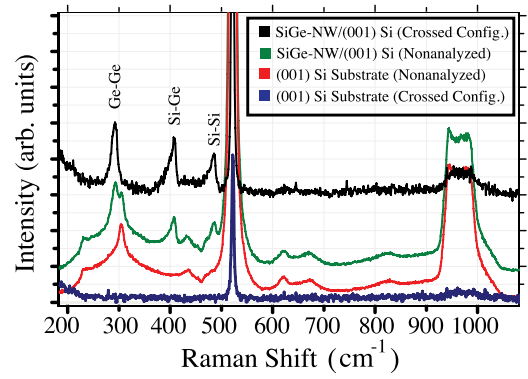
following equations:[24]

$$\omega_{SiSi} = 520.7 - 67x, \qquad (2)$$

$$\omega_{GeGe} = 280.3 + 19.4x. \qquad (3)$$

The Raman spectra revealed that the Ge composition was very close to the value estimated from elaboration conditions.[21,22] We also verified that x was constant over the NW length by recording spectra in the middle and near both extremities. Due to chemical disorder, inducing phonon peak asymmetry and strong background, and to the small influence of x on ω_{SiGe} for x close to 0.5, the precision on x cannot be better than a few percent.[25,26] This precision is sufficient however since such small composition changes have a limited impact on Q_{abs} and Q_{sca} (see Fig. 2, for instance).

In the following, we focus on four nanowires identified in Fig. 5 and in Table I.

Figure 7 presents the normalized experimental scattering spectra of NW47, NW49, NW74, and NW82. The normalization procedure to take into account the lamp spectrum and the spectrometer response is made using the following formula:

$$I(\lambda)_{normalized} = \frac{I(\lambda)_{NW} - I(\lambda)_{BG}}{I(\lambda)_{ref,on} - I(\lambda)_{ref,off}}, \qquad (4)$$

where $I(\lambda)_{NW}$ and $I(\lambda)_{BG}$ correspond to the intensity measured on and outside the NW, respectively. The reference $I(\lambda)_{ref,on} - I(\lambda)_{ref,off}$ is obtained by recording the light scattered by a white substrate with the lamp switched on [$I(\lambda)_{ref,on}$] and off ($I(\lambda)_{ref,off}$). All spectra are recorded in dark field configuration. Our results show that elastic light scattering from $Si_{1-x}Ge_x$ NWs is strongly enhanced for specific diameter-dependent

TABLE I. Diameter D, Length L, and composition x of the investigated individual $Si_{1-x}Ge_x$ nanowires.

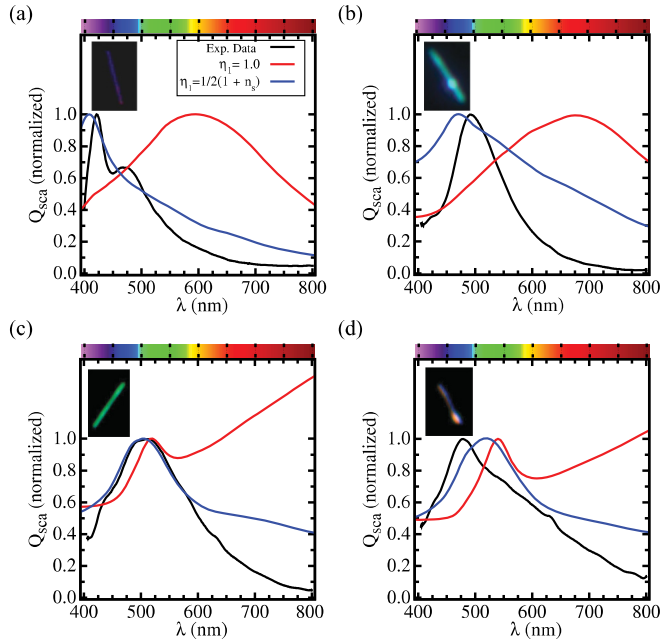|	D (nm)	L (μm)	x
NW47	47	1.9	0.22
NW49	49	5.5	0.54
NW74	74	6.5	0.55
NW82	82	6.9	0.50

FIG. 7. (Color online) Normalized experimental scattering spectrum (black line) of NW47 (a), NW49 (b), NW74 (c), and NW82 (d), compared to the scattering efficiency Q_{sca} of the same nanowire in two different dielectric environments (red line for vacuum and blue line for an average medium taking account of the substrate, see text). The inset shows the dark field color image of the nanowire.

wavelengths at fixed x [Figs. 7(b)–7(d)], as well as for x-dependent wavelengths at fixed diameter [Figs. 7(a)–7(b). We then compare our experimental results to numerical simulations of Q_{sca} based on the optical refractive index of $Si_{1-x}Ge_x$ alloys in which x is the Ge composition measured by Raman spectroscopy. Both experiments and calculations refer to the case of an unpolarized incident light.

The direct comparison between experiment and theory for a nanowire in vacuum ($\eta_1 = 1$) does not lead to a satisfactory agreement. Obviously, the origin for these differences can arise from the contribution of the underlying silicon substrate. To take into account the substrate, we assume that the NW is placed in a nonabsorbing medium with a refractive index $\eta_1 = (1 + n_s)/2$, given by the average between the vacuum refractive index and the silicon refractive index n_s. In first approximation, silicon can be considered as a nonabsorbing material in the 400–800-nm range of our scattering experiments. The Si extinction coefficient k stays below 0.02 except from about 400–450 nm, where it increases up to 0.4.

As can be seen in Fig. 7, there is a good agreement with the experimental spectra when correcting the index of the surrounding medium in Lorenz-Mie theory. In the case of NW47 and NW49, the resonance corresponding to the TM_{01} mode in the effective medium is strongly blueshifted compared to the same NW in air. In the case of NW74 and NW82, the short-wavelength mode, which is a degenerated TM_{11}/TE_{01}, is less affected by the surrounding medium. On the other hand, the resonance at larger wavelength seems to be damped and shifted when changing the surrounding medium index from 1 to $(1 + n_s)/2$. This resonance, also corresponding to the lowest-order mode TM_{01}, is expected to have a larger

extent outside the NW than the higher-order mode at shorter wavelength, which is more confined in the NW and thus less sensitive to its environment. This behavior was reported by Cao *et al.*, who emphasized a better agreement between theory and experiment for higher-order modes when several modes are observed.[6] It can also be seen in the insets of Fig. 4 exhibiting the normalized electric-field intensity for different modes. The electric-field extension outside the NWs decreases with increasing order, for instance from TM_{11} to TM_{13}.

The analytic Lorenz-Mie theory is thus interesting to find the LMRs wavelength of $Si_{1-x}Ge_x$ NWs, even for NWs deposited on high refractive index substrates, at least when small diameter NWs are considered. For a better agreement in modeling the real geometry of a nanowire (facetted, for instance) deposited on a high index and/or nontransparent substrate, the use of more sophisticated numerical methods would be useful. However, modeling the silicon substrate may not be trivial because of its low extinction coefficient in the visible spectrum. Recent finite-difference time-domain (FDTD) calculations have used either transparent substrates as glass[10,27] or metals,[13,27] for which huge absorption would limit the substrate thickness to a few nanometers.

IV. CONCLUSION

In this paper, we calculated the scattering and absorption efficiencies of $Si_{1-x}Ge_x$ nanowires using Lorenz-Mie theory, and taking into account the NW diameter and composition, light polarization, and angle of incidence. We have shown that the germanium composition provides an additional degree of freedom allowing us to tune light scattering and absorption over a broad spectral range from UV to infrared. High values of either Q_{sca} or Q_{abs} can be obtained with $Si_{1-x}Ge_x$ nanowire diameters compatible with CVD growth methods (20–250 nm). These one-dimensional nano-objects could provide interesting benchmarks for sensitive vibrational spectroscopies. Complementary Raman and dark field spectroscopy performed on individual nanowires have provided a clear evidence of both the composition and diameter-dependent enhanced optical response. Our experimental results on small diameter nanowires (50–80 nm) deposited on silicon substrates are in satisfactory agreement with the analytical Lorenz-Mie theory even using an average refractive index for the surrounding medium.

APPENDIX

1. Theoretical calculations

To investigate the optical properties of the nanowires, we have used the Lorenz-Mie theory. The nanowire (NW) is

supposed to be embedded in a linear, homogeneous, isotropic, nonabsorbing surrounding medium. We modeled a NW as an infinitely long cylinder of radius a. For this particular geometry, the analytical expression for the Laplacian operator is well known allowing us to solve the Helmholtz wave equation,

$$\Delta \mathbf{A} + k^2 \mathbf{A} = \mathbf{0}. \tag{A1}$$

The analytical solution of this equation is derived using the separation of variables method and then expanding the internal and external fields ($\mathbf{E},\mathbf{H}$) in vector cylindrical harmonics generated by the appropriate scalar wave functions. The external field includes the incident field and the scattered field. The expressions of the scattering and the absorption cross sections, related to the Poynting vectors, only depend on the expansion coefficients of the scattered field a_n and b_n. These coefficients can be deduced from the continuity of the tangential field components across the cylinder surface ($r = a$).

For an infinitely long cylinder, the corresponding cross sections are infinite. To overcome this problem, dimensionless quantities can be calculated. These quantities are obtained by dividing the optical absorption or scattering cross sections by the cylinder geometric cross section $2aL$.

The optical response of the system composed by the nanowire and its surrounding medium under slanting incidence is polarization dependent. The transverse magnetic (TM) and transverse electric (TE) efficiencies expressions are as follows:

$$Q_{\text{sca}}^{\text{TM}} = \frac{2}{\Omega}\left[|b_0^{\text{TM}}|^2 + 2\sum_{n=1}^{+\infty}\left(|a_n^{\text{TM}}|^2 + |b_n^{\text{TM}}|^2 \right) \right], \tag{A2}$$

$$Q_{\text{abs}}^{\text{TM}} = \frac{2}{\Omega}\mathbf{Re}\left\{ b_0^{\text{TM}} + 2\sum_{n=1}^{+\infty} b_n^{\text{TM}} \right\} - Q_{\text{sca}}^{\text{TM}}, \tag{A3}$$

$$Q_{\text{sca}}^{\text{TE}} = \frac{2}{\Omega}\left[|a_0^{\text{TE}}|^2 + 2\sum_{n=1}^{+\infty}\left(|a_n^{\text{TE}}|^2 + |b_n^{\text{TE}}|^2 \right) \right], \tag{A4}$$

$$Q_{\text{abs}}^{\text{TE}} = \frac{2}{\Omega}\mathbf{Re}\left\{ a_0^{\text{TE}} + 2\sum_{n=1}^{+\infty} a_n^{\text{TE}} \right\} - Q_{\text{sca}}^{\text{TE}}, \tag{A5}$$

where $\Omega = \frac{2\Pi a\eta_1}{\lambda}$ is the size parameter (η_1 is the surrounding host medium refractive index and λ is the vacuum wavelength value). The NW optical response under unpolarized illumination is the average between TM and TE:

$$Q_{\text{sca,abs}}^{\text{UP}} = \tfrac{1}{2}\left[Q_{\text{sca,abs}}^{\text{TM}} + Q_{\text{sca,abs}}^{\text{TE}} \right]. \tag{A6}$$

For non-normal incidence illumination and TM polarization, the scattering coefficients a_n^{TM} and a_n^{TM} are given below:

$$\mathbf{a_n^{\text{TM}}} = \frac{\mathbf{C_n V_n - B_n D_n}}{\mathbf{W_n V_n + i D_n^2}}, \quad \mathbf{b_n^{\text{TM}}} = \frac{\mathbf{W_n B_n + i D_n C_n}}{\mathbf{W_n V_n + i D_n^2}}$$

$$\mathbf{D_n = n\cos\xi \, \alpha J_n(\alpha) H_n^{(1)}(\beta)}\left(\frac{\beta^2}{\alpha^2} - \mathbf{1} \right)$$

$$\mathbf{B_n = \beta\left[\eta^2 \beta J_n'(\alpha) J_n(\beta) - \alpha J_n(\alpha) J_n'(\beta) \right]}$$

$$\mathbf{C_n = n\cos\xi \, \alpha J_n(\alpha) J_n(\beta)}\left(\frac{\beta^2}{\alpha^2} - \mathbf{1} \right)$$

$$\mathbf{V_n = \beta\left[\eta^2 \beta J_n'(\alpha) H_n^{(1)}(\beta) - \alpha J_n(\alpha) H_n^{(1)'}(\beta) \right]}$$

$$\mathbf{W_n = i\beta\left[\alpha J_n(\alpha) H_n^{(1)'}(\beta) - \beta J_n'(\alpha) H_n^{(1)}(\beta) \right]},$$
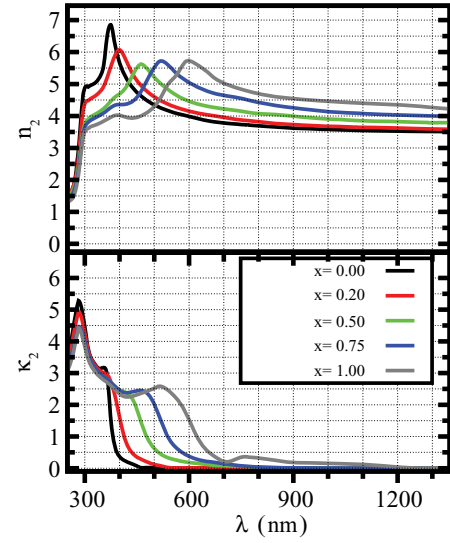
FIG. 8. (Color online) Real part n_2 and imaginary part κ_2 of the complex refractive index of $\text{Si}_{1-x}\text{Ge}_x$ for different germanium compositions.
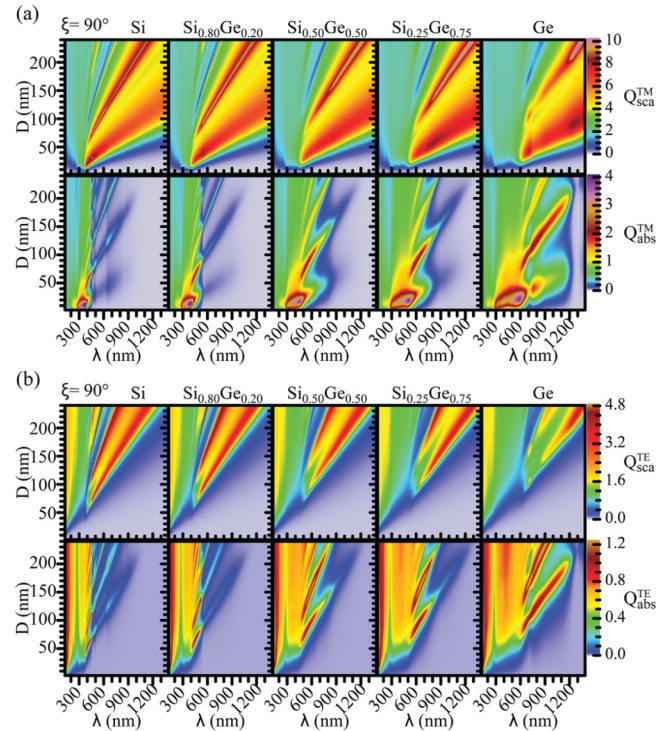
FIG. 9. (Color online) Scattering and absorption efficiencies of a $\text{Si}_{1-x}\text{Ge}_x$ NW in vacuum as a function of diameter and wavelength of incident light for different germanium compositions x. The incident wave vector is perpendicular to the cylinder axis. (a) TM polarized light, (b) TE polarized light.

where $\eta = \frac{\eta_2}{\eta_1}$ is the NW complex refractive index relative to the surrounding medium, $\beta = \Omega \sin \xi$ (ξ: angle of incidence), $\alpha = \Omega \sqrt{\eta^2 - \cos^2 \xi}$, J_n and $H_n^{(1)}$ are Bessel functions of the first kind and Hankel functions of the first kind, respectively. J_n' and $H_n^{(1)'}$ are the corresponding derivatives. More details about the Lorenz-Mie in the case of an infinite cylinder can be found, for example, in Ref. [15]

2. Optical constants of Si$_{1-x}$Ge$_x$ alloys

We have assumed that the complex refractive index $\eta_2 = n_2 + i\kappa_2$ for any alloy composition were that of relaxed bulk Si$_{1-x}$Ge$_x$. The missing data were interpolated from the optical constants measured by Humlícek and co-workers.[16,17] Figure [8] represents the real and imaginary part of the refractive index of Si$_{1-x}$Ge$_x$ for different germanium compositions. An increase in the Ge content clearly yields an overall redshift of the characteristic features such as the onset of the absorption due to direct electronic transitions from valence to conduction band.

3. Polarization dependence of light-scattering and absorption efficiencies

Figure [9] exhibits the dependence of Q_{sca} and Q_{abs} as a function of incident light polarization in normal incidence. Our results show that for any alloy composition, TM incident polarization allows more efficient light scattering and/or absorption compared to the TE polarization. Thus the chemical composition does not affect the polarization dependence of the Si$_{1-x}$Ge$_x$ nanowire optical response, which is in qualitative agreement with results obtained on pure Si NWs.[8] Furthermore, the selective investigation of TE and TM configurations allows us to identify the LMR resonances distributed on the (λ, d) maps of Fig. [2]. For instance, by comparing Figs. [9(a)] and [9(b)], one can notice that there is no corresponding TE branches for the TM$_{01}$ mode, this fundamental TM mode being nondegenerate. As detailed in the paper, it is the excitation of this TM$_{01}$ mode which governs the angular dependence of the optical response of small diameter nanowires. On the contrary, the higher-order TM$_{11}$ spectrally overlaps with the transverse electric TE$_{01}$ yielding a twofold degeneracy and a more complex optical response.

*houssem.kallel@cemes.fr

†Corresponding author: vincent.paillard@cemes.fr

[1] B. Tian, X. Zheng, T. J. Kempa, Y. Fang, N. Yu, G. Yu, J. Huang, and C. M. Lieber, Nature (London) **449**, 885 (2007).

[2] P. Yang, R. Yang, and M. Fardi, Nanolett. **10**, 1529 (2010).

[3] M. D. Kelzenberg, S. W. Boettcher, J. A. Petykiewicz, D. B. Turner-Evans, M. C. Putnam, E. L. Warren, J. M. Spurgeon, R. M. Briggs, N. S. Lewis, and H. A. Atwater, Nat. Mater. **9**, 239 (2010).

[4] O. L. Muskens, J. Gómez Rivas, R. E. Algra, E. P. A. M. Bakker, and A. Lagendijk, Nanolett. **8**, 2638 (2008).

[5] L. Cao, J. S. White, J.-S. Park, J. A. Schuller, B. M. Clemens, and M. L. Brongersma, Nat. Mater. **8**, 643 (2009).

[6] L. Cao, P. Fan, A. P. Vasudev, J. S. White, Z. Yu, W. Cai, J. A. Schuller, S. Fan, and M. L. Brongersma, Nanolett. **10**, 439 (2010).

[7] L. Cao, P. Fan, E. S. Barnard, A. M. Brown, and M. L. Brongersma, Nanolett. **10**, 2649 (2010).

[8] G. Brönstrup, N. Jahr, C. Leiterer, A. Csáki, W. Fritzsche, and S. Christiansen, ACS Nano **4**, 7113 (2010).

[9] G.-H. Ding, C. T. Chan, Z. Q. Zhang, and P. Sheng, Phys. Rev. B **71**, 205302 (2005).

[10] T. J. Kempa, J. F. Kahoon, S.-K. Kim, R. W. Day, H.-G. Park, and C. M. Lieber, Proc. Natl. Acad. Sci. USA **109**, 1407 (2012).

[11] L. Cao, B. Nabet, and J. E. Spanier, Phys. Rev. Lett. **96**, 157402 (2006).

[12] V. Poborchii, T. Tada, Y. Morita, T. Kanayama, and P. I. Geshev, Phys. Rev. B **83**, 153412 (2011).

[13] F. J. Lopez, J. K. Hyun, I. S. Kim, A. L. Holsteen, and L. J. Lauhon, Nanolett. **12**, 2266 (2012).

[14] L. Cao, B. Garipcan, E. M. Gallo, S. S. Nonnenmann, B. Nabet, and J. E. Spanier, Nanolett. **8**, 601 (2008).

[15] C. F. Bohren, D. R. Huffman, *Absorption and Scattering of Light by Small Particles* (John Wiley & Sons Inc., New York, 1998).

[16] J. Humlícek, M. Garriga, M. I. Alonso, and M. Cardona, J. Appl. Phys. **65**, 2827 (1989).

[17] J. Humlícek, *Properties of Silicon Germanium and SiGe:Carbon*, edited by E. Kasper and K. Lyutovich, EMIS Datareviews Series No. 24 (INSPEC, London, 2000), pp. 244–259.

[18] J.-E. Yang, C.-B. Jin, C.-J. Kim, and M.-H. Jo, NanoLett. **6**, 2679 (2009).

[19] J. Hu and C. R. Menyuk, Adv. Opt. Photon. **1**, 58 (2009).

[20] C. Penn, T. Fromherz, and G. Bauer, *Properties of Silicon Germanium and SiGe:Carbon* (Ref. [17]), pp. 125–134.

[21] A. Potié, T. Baron, F. Dhalluin, G. Rosaz, B. Salem, L. Latu-Romain, M. Kogelschatz, P. Gentile, F. Oehler, L. Montès, J. Kreisel, and H. Rousset, Nanoscale Res. Lett. **6**, 187 (2011).

[22] A. Potié, T. Baron, L. Latu-Romain, G. Rosaz, B. Salem, L. Montès, P. Gentile, J. Kreisel, and H. Rousset, J. Appl. Phys. **110**, 024311 (2011).

[23] I. Zardo, S. Conesa-Boj, F. Peiro, J. R. Morante, J. Arbiol, E. Uccelli, G. Abstreiter, and A. Foncuberta i Morral, Phys. Rev. B **80**, 245324 (2009).

[24] T. S. Perova, J. Wasyluk, K. Lyutovich, E. Kasper, M. Oehme, K. Rode, and A. Waldron, J. Appl. Phys. **109**, 033502 (2011).

[25] M. I. Alonso and K. Winer, Phys. Rev. B **39**, 10056 (1989).

[26] Q. Lu, K. W. Adu, H. R. Gutiérrez, G. Chen, K.-K. Lew, P. Nimmatoori, X. Zhang, E. C. Dickey, J. M. Redwing, and P. C. Eklund, J. Phys. Chem. C **112**, 3208 (2008).

[27] M. Heiss and A. Fontcuberta i Morral, Appl. Phys. Lett. **99**, 263102 (2011).